Draft version April 24, 2026
Typeset using LaTeX **default** style in AASTeX7

The Torpedo Bat: Physics or a Fad?

Nava Wolfish,[1] Alan M. Nathan,[2] and Erica Rosenblum[1]

[1] *University of Toronto*
[2] *University of Illinois, Urbana-Champaign*

ABSTRACT

In 2025, the New York Yankees pioneered the Torpedo bat, a novel bat shape that fit squarely within MLB guidelines. The new bat recentres mass from the tip of the bat to the sweet spot compared to the standrard bat. Since its introduction, many questions have been posed about whether the Torpedo bat has a measurable effect on batted balls. In this examination, we use Timoshenko beam theory and integrate with RK45 to simulate the bat-ball collision for both the standard and Torpedo using first-principles physics. We repeat these collisions for impact points across the barrel of the bat. We take an inelastic impacting ball with coefficent of restitution (COR) 0.5 and impact velocity of 44.704 m/s or 100 mph. We find that the Torpedo bat performs better at peak, yielding batted balls with an extra 1 mph. The highest difference in performance is 9.84 inches [25 cm] from the tip, where the Torpedo bat lends 2 mph more than the standard bat. We also observe the Torpedo bat has a wider sweet spot by 0.4 inches [1 cm], and that its sweet spot is shifted inwards on the bat. Additionally, we examine the differences in impacted force and bat-ball coefficient of restitution between both bats as a function of impact location. We conclude that the Torpedo bat does have measurable advantages over the standard bat. Further study is required on the partition of energy post-collision and new potential bat shapes.

1. INTRODUCTION

The most crucial moment in baseball occurs within a millisecond, when a batter swings at a pitch and hopes to make contact with the ball. If he does, the resulting collision induces complex energy and force profiles. The ball then flies off the bat at a determined angle and exit velocity, which results in an out (or two), a hit, or a home run. Throughout the history of Major League Baseball (MLB), restrictions have been placed on the bat's length, diameter, and material. However, there is a significant degree of flexibility in the bat shape and at which longitude the bat reaches its maximum diameter (Office of the Commissioner of Baseball 2026).

In 2025, Aaron Leanhardt pioneered a new bat shape, dubbed the Torpedo bat, with the New York Yankees. The bat recentres mass about 17 cm ($6\frac{1}{2}$ inches [16.5 cm]) from the tip at the "sweet spot" of the bat. Leanhardt's reasoning was that more mass behind the ball during the collision would yield higher exit velocities for batted balls. However, he predicted that the higher velocities would only hold for balls batted at the sweet spot, where the mass was refocused. In this examination, we determine if Leanhardt's hypothesis holds for the Torpedo bat using first-principles physics simulations. More broadly, we analyze if bat shape has a meaningful effect on batted ball results.

However, the key complication to our simulations is that the bat does not behave as a rigid body. It oscillates in response to a force according to the bat's stiffness, density, and shape. These oscillations are first described by L. L. Van Zandt (1992). Van Zandt discretizes the bat along its axis of symmetry into slices. Next, he derives expressions for the shear and normal forces on each slice imposed by its neighbours from first principles physics. His method closely resembles the Finite Element Method, and his equations of motion are consistent with the Timoshenko equation for a non-uniform elastic beam (J. N. Reddy 1993).

A. M. Nathan (2000) builds upon Van Zandt by including a model for the ball that accounts for energy loss in the collision. Nathan suggests the ball be described as an inelastic spring, whose energy loss is parametrized by a hysteresis curves. He is able to recreate controlled lab collision results for the exit velocity of a batted ball. Nathan analyzes the fractional energy contained within the bat, ball and the energy lost for a given set of collision parameters. Furthermore, he decomposes the bat's fractional energy into the energy contained in the bat's rigid motion and each of its normal modes. He finds that overwhelmingly, energy from the collision is lost due to imperfections in the ball.

However, the energy contained within bat vibrations has a steep minimum near the sweet spot of the bat, roughly 16 cm ($6\frac{1}{4}$ inches [15.9 cm]) from the tip. The location of the minimum accurately suggests a higher exit velocity for a batted ball near the sweet spot.

While we adopt the set of ordinary differential equations derived by Van Zandt and edited by Nathan, we also impose a set of boundary conditions to dictate how the knob and tip react to a collision. Clearly, the tip of the bat is free in a collision with the ball. However, the knob is held by the hands of the batter. R. Cross (1998) suggests that allowing the bat to be free on both ends is a sufficient approximation for the bat-ball collision. The timescales of the vibrations excited by the collision are much longer than the collision time. As a result, the wave in the bat does not reach the batters hands before the end of the collision. The motion of the bat on longer time scales is not the subject of interest for this paper, so it suffices to approximate the bat as free.

To integrate the ordinary differential equations of interest, we take a different approach than A. M. Nathan (2000) and L. L. Van Zandt (1992). Previous solutions have been determined in the modal space. In our simulations, we take a direct approach and integrate for the displacements and shears of each slice of the bat.

In this paper, we first present the bat-ball collision model and its governing equations. We then describe the simulation setup and parameter choices, followed by results for modal behavior, exit velocities, and collision dynamics. We conclude by interpreting what these results imply for the performance of Torpedo and standard bat geometries.

2. BAT-BALL COLLISION MODEL

The bat and the ball are coupled together through a set of ordinary differential equations. In this section, we describe independently the models for the bat and the ball and their equations of motion. We then illustrate how they combine to form the bat-ball collision. We also discuss a method for extracting the energy fractions contained in each degree of freedom within our system.

2.1. *The Bat*

We first consider only the oscillations of a free bat. In accordance with Nathan and Van Zandt, we model the baseball bat discretely as a Timoshenko beam. We align the main axis of symmetry of the bat with the z-axis, and slice the bat into N sections of thickness dz perpendicular to the axis (see Figure 1). Each slice of the bat has two degrees of freedom. A slice can displace from the equilibrium position normal to the z-axis and also angularly with respect to the normal. We establish coordinates such that ith slice has vertical displacement y_i and angular displacement ϕ_i. In our examination, we solve for $\Phi_i = \phi_i dz$ to maintain units of length. In total, our bat has $2N$ degrees of freedom.

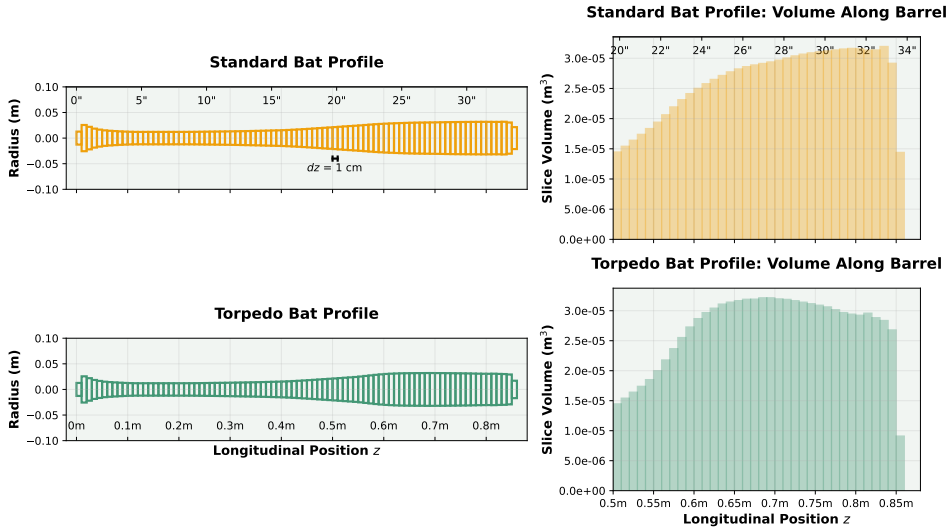

Figure 1. Radial profiles used to define the discretized bat geometry in both models. The top panel shows the standard bat profile and the bottom panel shows the Torpedo bat profile, while each vertical slice marks one numerical element of width $dz = 0.1$ cm. The Torpedo profile shifts radius, and therefore mass and inertia, toward the mid-barrel region relative to the standard profile.

Crucially, each bat has a measured longitudinal profile $\{R_i\}$, where R_i represents the cross-sectional radius of the ith slice of the bat. The batter's hands grasp the knob, or the 0th slice of the bat. The Nth slice is refered to as the tip. For a solid wooden bat, each slice has cross-sectional area $A_i = \pi R_i^2$ and moment of intertia $I_i = \pi R_i^4/4$ about the z-axis. Our examination also requires three observed parameters, Young's modulus Y_i, shear modulus S_i, and density ρ_i. A bat is required to be constructed from a singe wooden piece (Office of the Commissioner of Baseball 2026), so we take the reasonable approximation that these parameters are uniform. Henceforth, the subscripts are dropped, and we refer to these parameters as Y, S, ρ.

The set of oridinary differential equations are presented here without justification. L. L. Van Zandt (1992) thoroughly outlines his derivations of the motions of the bat, which are further improved upon by A. M. Nathan (2000). In accordance with their work, each bat slice i with displacement y_i and shear Φ_i oscillates freely as

$$\ddot{y}_i = \underbrace{\frac{S}{\rho(dz)^2}}_{\text{bat shear}} \left[\underbrace{y_{i+1} + y_{i-1} - 2y_i}_{\text{displacement from neighbours}} + \underbrace{\left(\frac{A_i - A_{i-1}}{A_i}\right)(y_i - y_{i-1} + \Phi_{i-1})}_{\text{correction for non-uniform cross-sections}} + \underbrace{(\Phi_i - \Phi_{i-1})}_{\text{dependence on rotation}} \right] \tag{1}$$

and

$$\ddot{\Phi}_i = \underbrace{\frac{Y}{\rho(dz)^2}}_{\text{bat stiffness}} \left[\underbrace{(\Phi_{i-1} + \Phi_{i+1} - 2\Phi_i)}_{\text{angular displacement from neighbours}} + \underbrace{\left(\frac{I_i - I_{i-1}}{I_i}\right)(\Phi_i - \Phi_{i-1})}_{\text{correction for non-uniform cross-sections}} \right] \tag{2}$$

$$- \underbrace{\left(\frac{S}{2\rho I_i}\right)}_{\text{bat shear}} \left[\underbrace{A_i(y_{i+1} - y_{i-1} + \Phi_i + \Phi_{i-1})}_{\text{shear induced torque}} - \underbrace{(A_i - A_{i-1})(y_i - y_{i-1} + \Phi_{i-1})}_{\text{correction for non-uniform cross-sections}} \right].$$

These equations of motion can be rearranged into the matrix equation

$$\ddot{\vec{\psi}} = \mathbf{H}\vec{\psi} \tag{3}$$

where the vector $\vec{\psi}$ is a concatenation of all slice displacements and rotations

$$\vec{\psi} = \begin{bmatrix} y_1 \\ \vdots \\ y_N \\ \Phi_1 \\ \vdots \\ \Phi_N \end{bmatrix}. \tag{4}$$

The elements of the matrix $\mathbf{H}$ encode the coupling between neighbouring bat slices. Definitions of the elements of $\mathbf{H}$ and a visualization of matrix elements is supplied in Appendix A.

In our examination, we use RK45 to directly integrate the system in Equation 3. However, it is worth decomposing $\mathbf{H}$ into its eigenvector basis. An eigenvector Ψ_n satisfies

$$\ddot{\vec{\Psi}}_n = -\omega_n^2 \vec{\Psi}_n. \tag{5}$$

These eigenvectors correspond to the normal modes and frequencies of the bat. On the timescale of our collision (< 1 ms), we only expect the first few modes with the lowest frequencies to be excited. Since the eigenvectors $\vec{\Psi}_n$ form a complete and orthonormal basis, we can take

$$\vec{\psi} = \sum_n a_n(t)\vec{\Psi}_n. \tag{6}$$

Nathan and Van Zandt integrate for $a_n(t)$, $\dot{a}_n(t)$ in their investigations.

In the case that a bat is impacted by a force, we introduce a term in the right hand side of Equation 3. We let the bat be impacted at a single slice, although it is straightforward to generalize to the multi-slice case. For a bat impacted at slice k with force $F_k(t)$,

$$\ddot{\vec{\psi}} = \mathbf{H}\vec{\psi} + \mathbf{M^{-1}}\vec{F}(t) \tag{7}$$

where

$$\vec{F}(t) = \begin{bmatrix} 0 \\ \vdots \\ F_k(t) \\ \vdots \\ 0 \end{bmatrix}. \tag{8}$$

The vector $\vec{F}(t)$ is zero except for the kth term, which contains the force magnitude. The matrix $\mathbf{M}$ is the mass matrix for the bat. It is a diagonal matrix with

$$M_{ii} = \begin{cases} \rho A_i dz & 1 \leq i \leq N \\ \frac{\rho I_i}{dz} & N \leq i \leq 2N \end{cases}. \tag{9}$$

2.2. *The Ball*

The ball is significantly inelastic, so quantifying its force on the bat requires prior knowledge of energy-loss parameters. We use the coefficient of restitution (COR) e_0, which parametrizes the energy lost in a collision with an immovable rigid body. If the ball impacts such a body with speed v_i and exits with speed v_f, then e_0 represents the ratio

$$e_0 = \frac{v_f}{v_i}. \tag{10}$$

Values of e_0 for a baseball are typically around $e_0 \approx 0.5$. The energy dissipated in the collision is

$$E_{\text{lost}} \propto v_i^2 - v_f^2 \propto 1 - e_0^2. \tag{11}$$

The ball compresses and expands in response to a force. So, in accordance with R. Cross (1999), we model the ball as a nonlinear spring. We define the ball's compression as u, measured with respect to its natural radius R_{ball}. We also define y_{ball} to be the position of the ball's centre of mass. We assume the ball compresses symmetrically during a collision.

Since the ball is inelastic, it compresses and expands along two different force profiles, F_c and F_e. Together, they form the closed loop $F(u)$. Then, the energy lost is

$$E_{\text{lost}} = \oint F(u)du \propto 1 - e_0^2. \tag{12}$$

The ball compresses according to

$$F_c = k_c u^{\alpha}. \tag{13}$$

Clearly, $\alpha = 2$ would result in an elastic spring. The value of α is determined experimentally, and has a typical value of ≈ 1.5 for a baseball. k_c represents the stiffness of the ball, with typical values for a baseball on the order of 10^7 N/m$^{\alpha}$. Similarly, the ball expands along

$$F_e = k_e u^{\beta}. \tag{14}$$

To preserve the relationship in Equation 12,

$$\beta = \frac{1+\alpha}{e_0^2} - 1. \tag{15}$$

Lastly, k_e is evaluated to preserve continuity at the maximum compression $u_{\max}$

$$k_e = k_c u_{\max}^{\alpha/\beta}. \tag{16}$$

The resulting hysteresis curve defines the force exerted on a bat slice during a collision. The ball begins with $u = 0$, $\dot{u} > 0$, and $F_k(t) = F_c(u)$ while the ball is squishing against the bat. The ball stops compressing when $\dot{u} = 0$, and the force switches to $F_k(t) = F_e(u)$. When $u = 0$, $\dot{u} < 0$, the ball returns to its natural radius and $F_k(t) = 0$. We define the collision time t_{coll} as the time at which the force decays to 1% of the maximum impact force. Note the collision time is distinct from the time the ball and the bat separate. Since the impacted slice displaces, the force goes to 0 while the bat and ball are still in contact.

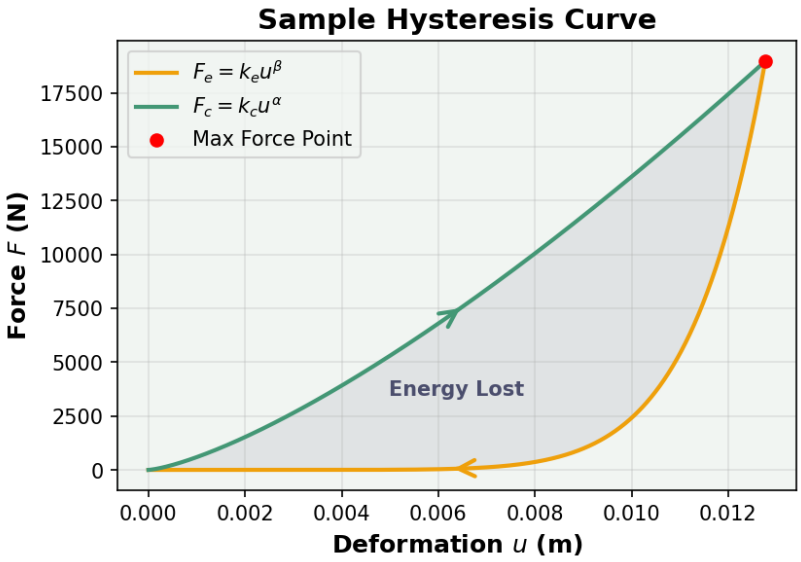

Figure 2. Sample hysteresis curve typical of a baseball. The green curve gives the force for a compressing ball, the yellow curve gives the force for an expanding ball, and the red dot marks the maximum force where the two branches join. The area between both curves is the energy lost in the collision, which constitutes a significant fraction of the initial energy.

The ball's equation of motion is then

$$\ddot{y}_{\text{ball}} = -\frac{1}{m_{\text{ball}}} F(u(t)), \tag{17}$$

since the force is negative pushing away from the bat.

2.3. *Bat and Ball Coupling*

We have independently determined the equations of motion for both the bat and the ball. They are coupled through the ball's compression, which is the difference between the ball's natural radius and the space between the ball's centre of mass y_{ball} and the slice position y_k. For an impact on the kth slice of the bat, the complete system is as follows:

$$\ddot{\vec{\psi}} = \mathbf{H}\vec{\psi} + \mathbf{M}^{-1}\vec{F}(t) \tag{18}$$

$$\ddot{y}_{\text{ball}} = -\frac{1}{m_{\text{ball}}} F_k(u(t)) \tag{19}$$

$$u(t) = R_{\text{ball}} - (y_{\text{ball}}(t) - y_k(t)) \tag{20}$$

We set the bat to be initially at rest, $\vec{\psi} = 0$. The ball begins in contact with the bat at $u = 0$, $y_{\text{ball}} = R_{\text{ball}}$. Note that

$$\dot{u}(t) = -\dot{y}_{\text{ball}}(t) - \dot{y}_k(t), \tag{21}$$

which is required to determine the relevant force at a given time.

2.4. *Rigid Expectation*

We compare our results with the non-rigid bat model to the rigid expectation. A. M. Nathan (2003) outlines the process for obtaining the rigid body expectation for the bat-ball collision. For a free bat, conservation of momentum assigns the bat an effective mass

$$\frac{1}{M_{\text{eff}}} = \frac{1}{M} + \frac{(z - z_{\text{cm}})^2}{I_{\text{cm}}} \tag{22}$$

which accounts for both translation and rotation. Equation 22 takes M as the bat's actual mass, z as the impact location, z_{cm} as the bat's centre of mass, and I_{cm} as the moment of inertia about the bat's centre of mass. We define the bat recoil factor r according to

$$r = \frac{m_{\text{ball}}}{M_{\text{eff}}}. \tag{23}$$

The bat-ball coefficient of restitution e (BBCOR) describes the difference between simulated v_f/v_i and the rigid bat expectation. It is given by

$$e = \left(\frac{v_f}{v_i}\right)(1 + r) + r. \tag{24}$$

BBCOR is a property of the geometry and composition of the bat and ball, independent of swing kinematics. As such, e is a better diagnostic for the efficiency of a collision compared to e_0 or v_f/v_i.

3. SIMULATION SET UP

Our main simulation compares the exit velocities of batted balls for both the standard and Torpedo bats as a function of longitudinal impact location. The bats differ in shape, and all other parameters are roughly equal within their orders of magnitude. The shapes are plotted in Figure 1. Our chosen parameters reflect true measurements of bat stiffness, shape, and mass by experimentalists like Cross. The ball parameters and impact speed are constant across all impacts. Our complete process is as follows:

1. Take the parameters for each bat outlined in Table 1.

	Standard	**Torpedo**	**Units**
Bat Length	86	86	cm
mass	890.175	908.319	g
Mass Density (ρ)	690	690	kg / m^3
Young's Modulus (Y)	1.64	1.65	$\times 10^{10}$ N / m
Shear Modulus (S)	10	9	$\times 10^{8}$ N / m
Slice Thickness (dz)	0.01	0.01	m
Number of Slices (N)	86	86	

Table 1. Bat parameters used across the simulations. The Standard and Torpedo columns give the two bat geometries being compared, and the Units column identifies the physical units for each row. The two bats are nearly identical in mass, material properties, and discretization, but differ in shape.

2. Take the parameters for the ball outlined in Table 2. Note the expansion stiffness k_e is not constant acrosss the collisions. The value of k_e is independently determined during each simulation when the ball reaches maximum compression $u_{\max}$ to ensure continuity of the hysteresis curve.

3. Select the impact index k.

4. Initialize the ball and bat to the initial conditions below. We take $v_i = 44.704$ m/s $= 100$ mph, which is a high but not anomalous MLB pitch velocity.

$$\vec{\psi}(t = 0) = 0 \qquad \dot{\vec{\psi}}(t = 0) = 0 \tag{25}$$

$$y_{\text{ball}}(t = 0) = R_{\text{ball}} \qquad u(t = 0) = 0 \tag{26}$$

$$\dot{y}_{\text{ball}} = v_i \tag{27}$$

Parameter	Value	Unit
Mass (m_{ball})	146	g
Natural Radius (R_{ball})	3.6600	cm
COR (e_0)	0.5	dimensionless
Compression Stiffness (k_c)	7.14	$\times 10^6$ N / m$^\alpha$
Compression Non-Linearity (α)	1.36	dimensionless
Expansion Non-Linearity (β)	8.44	dimensionless

Table 2. Ball parameters used in the collision model. The table lists the baseball mass and natural radius in the first two rows, and the remaining rows specify the compression-rebound law through the restitution and spring parameters that govern how much energy is lost during collision.

5. Use RK45 to integrate the collision for 2 ms with a timestep $h = 2\mu$s. After each step, check the most recent values of $\dot{u}$ and u to determine the relevant force profile $F_k(t)$.
   (a) When $\dot{u} = 0$ and $u > 0$, then the force profile switches from $F_c \to F_e$. Store the maximum compression and force values. Calculate the expansion stiffness k_e according to Equation 16.
   (b) When F_e is less than 1% of $F_{\max}$, store the corresponding time as $t_{\text{collision}}$.
   (c) When $\dot{u} < 0$ and $u = 0$, let $F_k \to 0$. Store current value of $|\dot{y}_{\text{ball}}|$ as the exit velocity v_f.
6. After the bat and ball separate, the ball flies with constant velocity v_f and the bat oscillates freely.
7. Reset the bat and ball solutions. Repeat steps 3-6 for $50 \leq k < N$ across the barrel of the bat.

4. RESULTS

4.1. *Modal Analysis*

Before we perform the simulations outlined in Section 3, we first analyze the normal modes and frequencies of the bats. The normal modes encode significant geometrical features of each bat. Understanding the location of the nodes of each mode informs why the ball's exit velocity changes as a function of impact location. Table 3 contains the 6 lowest normal frequencies for both bats. The Torpedo frequencies shift slightly higher than the standard frequencies. This shift corresponds to marginally shorter timescales for the Torpedo bat's ocsillations.

Mode	Standard Frequency (Hz)	Standard Period (ms)	Torpedo Frequency (Hz)	Torpedo Period (ms)
Mode 1	141.88	7.05	143.14	6.99
Mode 2	505.36	1.98	509.16	1.96
Mode 3	1036.55	0.96	1050.91	0.95
Mode 4	1625.55	0.62	1645.98	0.61
Mode 5	2296.50	0.44	2296.55	0.44
Mode 6	3010.61	0.33	2979. 03	0.34

Table 3. Lowest normal-mode frequencies and corresponding periods for the standard and Torpedo bats. The table is read left to right as mode number, standard-bat frequency and period, and Torpedo-bat frequency and period, and the Torpedo modes are slightly higher in frequency so they oscillate on marginally shorter timescales than the standard bat.

We also plot the normal mode shapes for both bats in Figure 3. The modes barely differ between the standard and Torpedo bats. However, the modes for the Torpedo bat fall slightly inside the standard bat modes along the barrel, with $z \geq 0.5$m. For both bats, the first mode has a node at $z = 0.68$ cm, or 6.7 inches [17.0 cm] from the tip of the bat. The second mode has a node at $z = 0.75$ cm, or 5.1 inches [13.0 cm] from the tip of both bats. Since the first two modes contain timescales longer than our collision, we expect they will constitute the majority of our vibrations. If the ball hits a node, the corresponding mode will not be excited in the collision. So, we expect collisions on the bats between $z = 0.68$ cm and $z = 0.75$ cm to transfer the least amount of energy to bat vibrations, and hence more energy will be transfered to the ball.

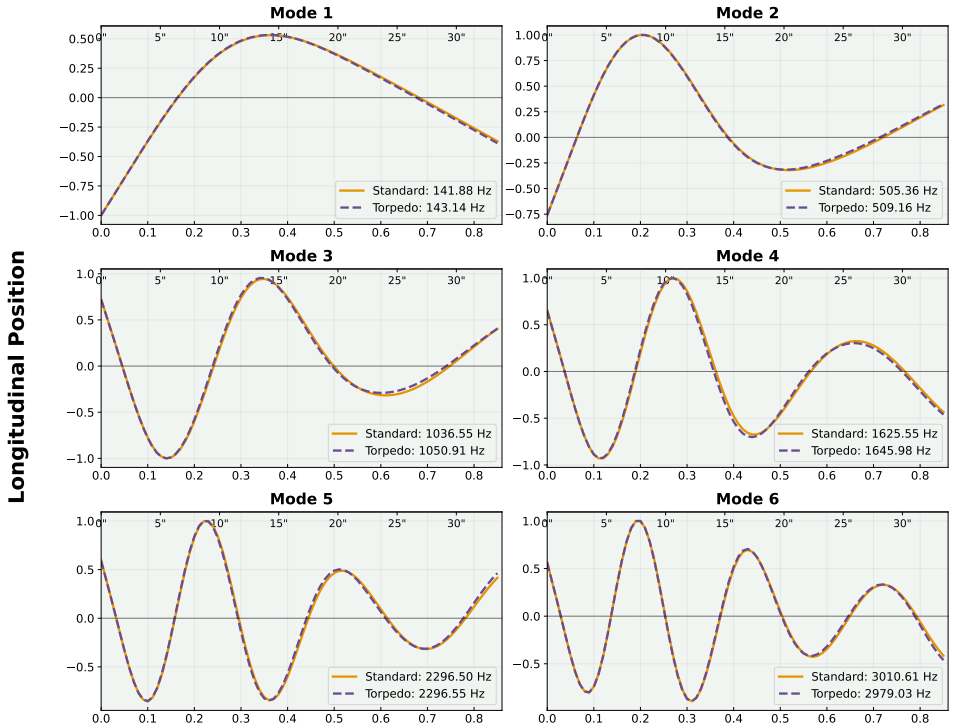

Figure 3. Normal mode shapes for the standard and Torpedo bats. Each figure plots a single mode for the standard (in yellow) and Torpedo (dashed purple) bats. The standard-bat and Torpedo-bat curves lie nearly on top of each other. The small inward shift of the Torpedo curves along the barrel helps explain why its peak collision response also shifts toward the knob.

4.2. *Exit Velocities*

After running our simulations, we examine the fraction v_i/v_f for the ball over each collision. We formally define the sweet spot as the region where v_f/v_i is greater than the combined 80th percentile limit over all exit velocities (including both bats). For our simulations, the sweet spot is where $v_f/v_i \geq 0.22$.

The results our simulation are shown in Figure 4. We notice that the curve for the Torpedo bat is shifted inwards on the bat (closer to the knob) compared to the standard bat. We also notice the Torpedo bat yields marginally higher exit velocities, especially at the sweet spot. As expected, the range for $v_f/v_i < e_0 = 0.5$, because some of the initial kinetic energy of the ball is transfered to the bat's rigid motion and its vibrations.

Interestingly, the sweet spot of the Torpedo bat is wider than the sweet spot of the standard bat by 1 cm or 0.4 inches [1.0 cm]. The sweet spot for the standard bat ranges from $5.91 - 8.26$ inches [15.0–21.0 cm] from the tip, while the sweet spot for the Torpedo bat ranges from $5.91 - 8.66$ inches [15.0–22.0 cm] from the tip. So, both sweet spots start at the same location on the outside of the bat, but the Torpedo has a higher production value as the collisions progress towards the knob.

The velocity increase for the Torpedo bat is minimal but apparent. The average fractional increase in velocity with the Torpedo bat is 0.0038 per bat collision. The difference in performance is clearest 9.84 inches [25.0 cm] from the tip, where the Torpedo bat contributes an fractional increase of 0.0196, or an extra 2 mph for our impact at $v_i = 100$ mph. The maximum velocities attained by both bats differ by 0.0088, or ≈ 1 mph for our pitch.

4.3. *Compression and Force*

We now examine the maximum force induced between the bat and ball across all collision locations. A plot of these findings is shown in Figure 5. For both bats, the maximum force rises sharply as the impact location moves from the tip to the knob. Both bats have the maximum induced force on the outside (leftmost) edge of their sweet spot, before steadily declining along the barrel. In the sweet spot and towards the barrel, the maximum force induced on the Torpedo bat is higher than the standard. Near the tip, the standard bat experiences a higher maximum force compared to the Torpedo.

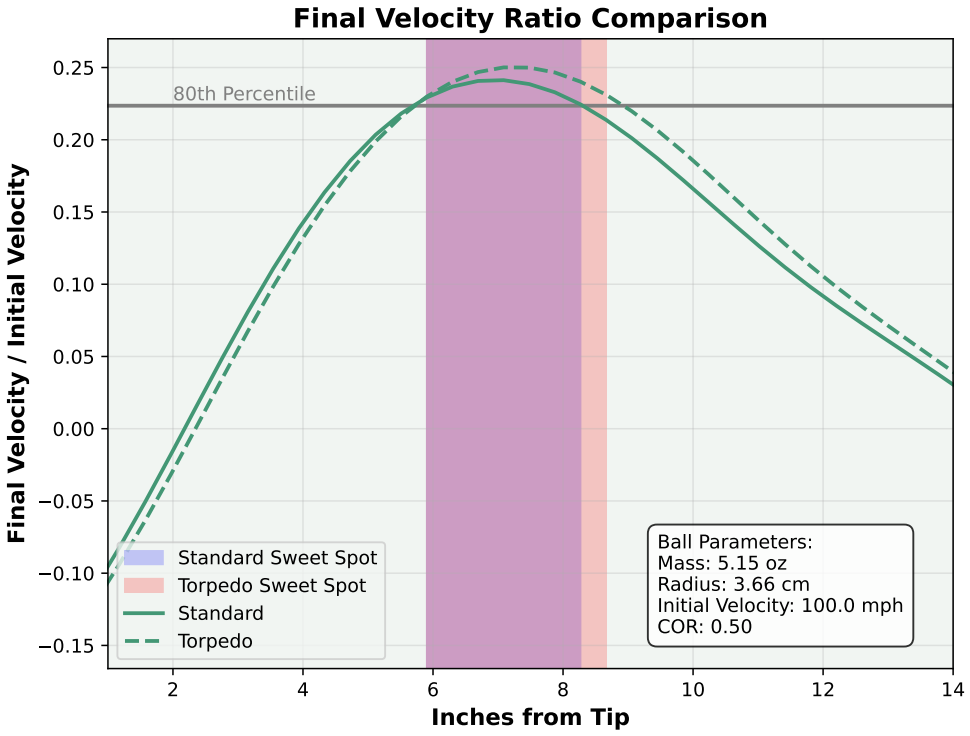

Figure 4. Exit velocity as a function of impact location for the standard and Torpedo bats. The Standard-bat curve and Torpedo-bat curve trace the simulated exit-speed ratio along the barrel, and the Torpedo curve sits slightly higher through the sweet spot while shifting the best-performing region inward toward the knob.

4.4. *Bat-Ball Coefficient of Restitution*

Finally, we discuss the bat-ball coefficent of restitution defined in Equation 24. The values of r, e, and v_f/v_i across the barrel are shown in Figure 6. As expected, since r depends on the difference between the bat's centre of mass and collision location, it decreases monotonically across the barrel. The overall effect on e is to shift its shape toward the tip in comparison to v_f/v_i. Since r is nearly the same for the Torpedo and the standard bats, the difference in e is accounted wholy by our simulations. Despite the subtle difference in geometry, the propogating effects from v_f/v_i to e are significant.

At maximum, both bats have the same maximum e within 1 cm of the same bat location. When it comes to inhibiting energy lost to the bat vibrational modes, both bats have nearly identical effects at peak. However, the Torpedo bat has strictly higher e inside the peak and the standard bat has strictly higher e outside the peak.

5. DISCUSSION

In this paper, we simulate the collisions between a baseball and two different baseball bat shapes. We compare a standard baseball bat with a steadily increasing radius to the Torpedo bat that recentres mass towards the sweet spot. We model both bats as non-uniform Timoshenko beams in accordance with A. M. Nathan (2000) and L. L. Van Zandt (1992). The bats are split into discrete slices, each with one translational and one rotational degree of freedom. We model the ball as an inelastic spring and discuss the hysteresis curves associated with ball collision. Then, we discuss the rigid body expectations to inform the definition of e, the bat-ball coefficient of restitution.

We impact a 100 mph ball at each bat, iterating the impact location for each collision along the bat barrel. We employ a RK45 integrator and integrate each solution for 2 ms with a timestep of 2μs. Notably, the only relevant differences between our bats is their shape, as we take similar values for bat stiffness and density. We use a ball with a coefficent of restitution of 0.5, implying the energy lost in a collision with an immovable rigid body is proportional to $1 - e_0^2$.

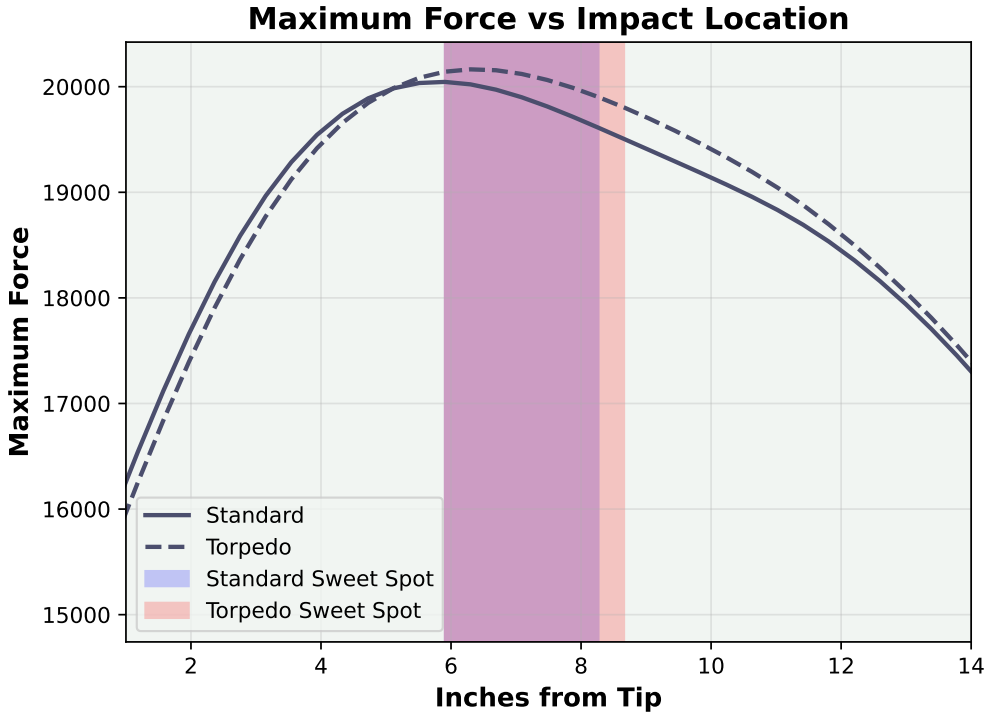

Figure 5. Maximum bat-ball force as a function of impact location for both bats. The Standard-bat and Torpedo-bat curves show the largest force reached during each collision, with impacts closer to the knob producing stronger forces overall and the Torpedo bat running slightly higher through the interior portion of the barrel.

We obtain significant differences in standard and Torpedo bat performances. The three main findings of our simulation are that the Torpedo bat has

- higher exit velocities on average, with a peak gain of 2mph over the standard bat for a 100mph pitch;
- a sweet spot shifted inside on the bat towards the knob;
- and a wider sweet spot than the standard bat by 0.4 inches [1.0 cm].

Both bats had peak fractional exit velocity 6-8 inches [15.2–20.3 cm] from the tip of the bat. Interestingly, this peak is shifted inside on the bat compared to node placement of the first two lowest vibrational modes.

The three main findings (higher, inside, wider) for the Torpedo bat are also consistent with the maximum force impacted in both collisions. However, the BBCOR for both bats have the same peak magnitude. We observe the Torpedo bat has higher collision efficiency inside the sweet spot while the standard bat performs better outside the sweet spot.

These findings are significant within the context of a Major League Baseball game. Many fly balls are caught as outs at the back of the outfield. An increase in exit velocity of 1-2 mph could transform many of these fly balls into home runs. Hitters that consistently hit the ball inside the bat's sweet spot may find better performance with the Torpedo bat. Moreover, hitters that hit the sweet spot less consistently may find better performance on average with the Torpedo bat. The MLB landscape at present is heavily biased towards any analytical insights that can increase performance. Even small changes in gameplay can turn a struggling team into a World Series contender. Our findings indicate that studying the shape of the bat can provide the competitive edge that every MLB team yearns for.

While our conclusions are promising, there are important caveats to consider when applying our studies to the baseball field. We only consider a non-rotating, spherically symmetrical bat being hit squarely with the baseball. We do not consider oblique collisions. In reality, the baseball is highly asymmetrical. The portruding ball seams have an overwhelming effect on ball flight and collisions due to the turbulence and drag effects (J. R. Kensrud et al. 2015).

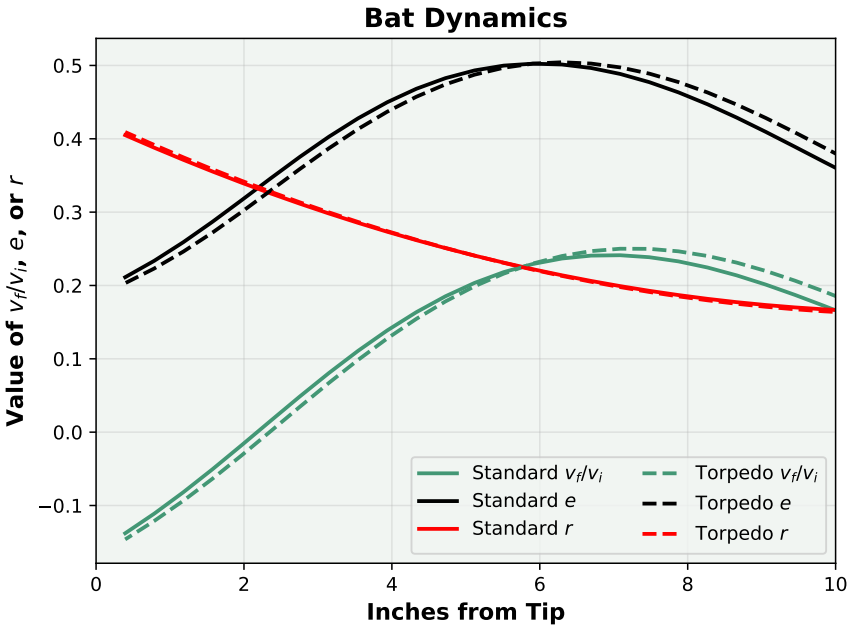

Figure 6. Bat-ball coefficient of restitution, recoil factor, and simulated exit-speed ratio across impact locations on the barrel. The plotted curves track how the recoil factor and exit-speed ratio vary together along the bat, and the Torpedo bat performs slightly better inside the sweet spot while the standard bat is marginally stronger outside it.

The baseball is also always spinning, as the combination of seam orientation and spin differentiates pitch types. It is rare that our controlled results could be replicated identically in gameplay. However, our observed trends should hold.

Further study would involve finding the fractional energies contained within the bat, ball, each vibrational mode, and the energy dissipated as heat. Another study could examine additional bat shapes, and aim to tailor the shape of the bat to a hitter's swing profile.

APPENDIX

A. MATRIX COMPONENT TABLES

This appendix elaborates on the matrix **H** and its composition. We can imagine **H** as a concatenation of four quadrants, each describing how a $\ddot{\psi}_i$ component depends on a first-order term. The first quadrant relates $\ddot{y}_i$ to y_k, the second relates $\ddot{y}_i$ to Φ_k, the third relates $\ddot{\Phi}_i$ to y_k, and the fourth relates $\ddot{\Phi}_i$ to Φ_k (See Figure 7). Since each slice is only coupled to its neighbours, we expect each quadrant of **H** to be tridiagonal.

First, we define

$$\Lambda \equiv \frac{S}{\rho(dz)^2} \qquad\qquad \Upsilon \equiv \frac{Y}{\rho(dz)^2}. \tag{A1}$$

We consider the rows $i \in \{2, 3, ..., N-1\}$. These rows are the central rows of **H** and are independent of the boundary conditions imposed on the bat. We also let $j = i + N$ as an index for quadrants 2, 3, and 4. We obtain components of **H** from Equations 1 and 2, as outlined in Table 4.

Next, we consider the edges of each quadrant. Invoking our boundary conditions, we obtain the components outlined in Table 5.

All other components of **H** are uniformly zero.

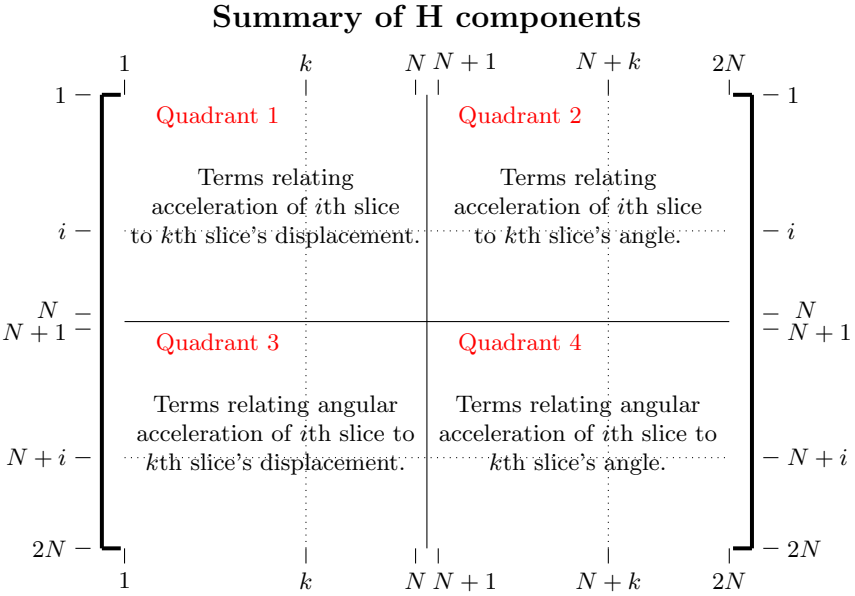

Figure 7. Block-structure schematic for the system matrix **H** in the coupled bat equations of motion. Quadrant 1 maps translational acceleration $\ddot{y}_i$ to displacement y_k, Quadrant 2 maps $\ddot{y}_i$ to angular displacement Φ_k, Quadrant 3 maps angular acceleration $\ddot{\Phi}_i$ to y_k, and Quadrant 4 maps $\ddot{\Phi}_i$ to Φ_k; dotted guides indicate index ranges across the $2N \times 2N$ matrix. This layout shows that translation and rotation are fully coupled and that each block is tridiagonal because each slice interacts only with neighboring slices.

ACKNOWLEDGMENTS

REFERENCES

Cross, R. 1998, American Journal of Physics, 66, 772, doi: 10.1119/1.19030

Cross, R. 1999, American Journal of Physics, 67, 692, doi: 10.1119/1.19354

	Quadrant 1	**Quadrant 2**
Diagonal	relevant indices $\{(i,i)\}$	relevant indices $\{(i,j)\}$
Upper	$H_{i,i+1} = \Lambda$	$H_{i,j+1} = \dfrac{\Lambda}{2}$
Main	$H_{i,i} = -\Lambda\left(1 + \dfrac{A_{i-1}}{A_i}\right)$	$H_{i,j} = \dfrac{\Lambda}{2}\left(1 - \dfrac{A_{i-1}}{A_i}\right)$
Lower	$H_{i,i-1} = \Lambda\dfrac{A_{i-1}}{A_i}$	$H_{i,j-1} = -\Lambda\dfrac{A_{i-1}}{2A_i}$
	Quadrant 3	**Quadrant 4**
Diagonal	relevant indices $\{(j,i)\}$	relevant indices $\{(j,j)\}$
Upper	$H_{j,i+1} = -\Lambda\dfrac{A_i(dz)^2}{2I_i}$	$H_{j,j+1} = \Upsilon - \Lambda\dfrac{A_i(dz^2)}{4I_i}$
Main	$H_{j,j} = -\Upsilon\left(1 + \dfrac{I_{i-1}}{I_i}\right) - \Lambda\dfrac{A_i(dz)^2}{4I_i}\left(1 + \dfrac{A_{i-1}}{A_i}\right)$	
Lower	$H_{j,i-1} = \Lambda\dfrac{A_{i-1}(dz)^2}{2I_i}$	$H_{i,j-1} = -\Upsilon\left(\dfrac{I_{i-1}}{I_i}\right) - \Lambda\dfrac{A_i(dz)^2}{4I_i}$

Table 4. Central (interior-slice) coefficient definitions for the system matrix **H**. The table is organized by diagonal type in the rows, by quadrant block in the columns, and each entry gives the nonzero coefficient for an interior index $i \in \{2, \ldots, N-1\}$. All interior couplings are nearest-neighbor and parameterized by local area and inertia ratios, producing a sparse tridiagonal block structure.

Felippa, C. A. 2004,

Hendee, S. P., Greenwald, R. M., & Crisco, J. J. 1998, Journal of Applied Biomechanics, 14, 390, doi: 10.1123/jab.14.4.390

Kensrud, J. R., Smith, L. V., Nathan, A., & Nevins, D. 2015, Procedia Engineering, 112, 406, doi: 10.1016/j.proeng.2015.07.216

Nathan, A. 2025,

Nathan, A. M. 2000, American Journal of Physics, 68, 979, doi: 10.1119/1.1286119

Nathan, A. M. 2003, American Journal of Physics, 71, 134, doi: 10.1119/1.1522699

Nathan, A. M. 2025,

Office of the Commissioner of Baseball. 2026, Office of the Commissioner of Baseball

Passan, J. 2025,, https://www.espn.com/mlb/story/_/id/44477141/mlb-2025-torpedo-bowling-pin-bats-new-york-yankees-taking-baseball ESPN

Reddy, J. N. 1993, An Introduction to the Finite Element Method, 2nd edn., McGraw-Hill Series in Mechanical Engineering (New York: McGraw-Hill)

Van Zandt, L. L. 1992, American Journal of Physics, 60, 172, doi: 10.1119/1.16939

	Quadrant 1	**Quadrant 2**
Boundary	relevant indices $\{(i,i)\}$	relevant indices $\{(i,j)\}$
Knob	$H_{1,1} = -\Lambda$	$H_{1,N+1} = \dfrac{\Lambda}{2}$
	$H_{1,2} = \Lambda$	$H_{1,N+2} = \dfrac{\Lambda}{2}$
Tip	$H_{N,N-1} = \Lambda \dfrac{A_{N-1}}{A_N}$	$H_{N,2N-1} = -\Lambda \dfrac{A_{N-1}}{2A_N}$
	$H_{N,N} = -\Lambda \dfrac{A_{N-1}}{A_N}$	$H_{N,2N} = -\Lambda \dfrac{A_{N-1}}{2A_N}$
	Quadrant 3	**Quadrant 4**
Boundary	relevant indices $\{(j,i)\}$	relevant indices $\{(j,j)\}$
Knob	$H_{N+1,1} = -\Lambda \dfrac{A_N (dz)^2}{4I_N}$	$H_{j,j+1} = \Upsilon - \Lambda \dfrac{A_i (dz^2)}{4I_i}$
Main	$H_{j,i} = \Lambda \dfrac{A_i (dz)^2}{2I_i} \left(1 - \dfrac{A_{i-1}}{A_i}\right)$	$H_{j,j} = -\Upsilon \left(1 + \dfrac{I_{i-1}}{I_i}\right) - \Lambda \dfrac{A_i (dz)^2}{4I_i} \left(1 + \dfrac{A_{i-1}}{A_i}\right)$

Table 5. Boundary (knob and tip) coefficient definitions for the system matrix **H**. The table groups the boundary rows by knob and tip conditions across the same quadrant blocks used in the interior table, and the entries replace the interior formulas wherever free-end conditions modify the coefficients. These boundary corrections enforce physically consistent free-end force and torque behavior in the discretized bat model.